Check for updates

Epoxy-matrix polyaniline/*p*-phenylenediamine-functionalised graphene oxide coatings with dual anti-corrosion and anti-fouling performance†

Sara Fazli-Shokouhi, [ID] [a] Farzad Nasirpouri [ID] *[a] and Maasoumeh Khatamian [ID] [b]

This research work reports on the anti-corrosion and anti-fouling properties of epoxy (E) coatings reinforced with polyaniline (PANI)/*p*-phenylenediamine-functionalised graphene oxide (PGO) composites. The mass ratio of graphene oxide/*p*-phenylenediamine in any PGO was assumed to be 1 : 1, but different PANI–PGO composites containing various loadings of PGO were prepared. An ultrasonic-assisted *in situ* polymerization method was employed to produce PANI–PGO at low temperature (0 °C). Several analytical and microscopical techniques, *i.e.*, Fourier-transfer infrared (FTIR) spectroscopy, X-ray diffraction (XRD), and field emission scanning electron microscopy (FESEM), were used to confirm that PANI–PGO composites were successfully synthesized. The epoxy-based coatings (E/PANI–PGO (*x*), *x* = 0.05–0.4 g) were applied by brushing them onto carbon steel substrates, which exhibited dual anti-corrosion and anti-fouling performance. Electrochemical impedance spectroscopy (EIS) results show that E/PANI–PGO (0.2) has the highest corrosion resistance (8.87×10^6 Ω cm^2) after 192 h of immersion in 3.5 wt% NaCl amongst all the coatings compared with neat epoxy (1.00×10^4 Ω cm^2) and E/PANI (6.82×10^3 Ω cm^2). Efficient antifouling performance at the macroscopic level under simulated marine conditions was observed for the epoxy-based PANI–PGO coatings with a range of PGO compositions, in particular for the 0.1 and 0.2 g PGO coatings.

Introduction

Corrosion and its prevention place considerable costs on industrial and modern organizations.[1,2] The application of coatings on metal or alloy parts is known as a practical way to prevent surface degradation and corrosion.[3,4] Over recent years, coating systems and performances have been remarkably enhanced using the great potential of nanotechnology.[4] One of the most common examples is composite nanocoatings, where the quality of conventional coatings may be improved by making nanocomposites using a small amount of nanoparticles towards cost-effective coating materials. There have been several applications and properties exploited thus far for nanocoatings, such as antifog, anticorrosion, antibacterial, water-proof, and antifouling coatings.[5] The production methods of nanocoatings are diverse, and include electrochemical deposition, chemical precipitation, physical perception, laser method, and sol–gel, techniques.[4,5]

Biofouling is a kind of pollution that occurs when microorganisms, algae, and living creatures gather together on floating surfaces. Biofouling can be divided into two main groups: micro (bacteria and diatoms) biofilm and macro (macro-algae, tube-worms, bryozoans).[6,7] Fouling pollution can be controlled according to salinity, temperature, nutrient materials, flow rate, and the strength of sunlight irradiation.[8–11] Tributyltin, tributyltin oxides, or some metal oxides have been used as pesticide coatings in recent years. The application of these coatings has been paused because of their harm to animals and human beings, and their use has been forbidden by environmental protection and government policy makers.[8,12] In this decade, scientists have attempted to design unusual environmentally-friendly coatings that are beneficial to the environment.[6,7,12,13]

Graphene is a relatively newly discovered material that has fantastic properties for scientific and technological goals and applications. Graphene is composed of a honeycomb structure of carbon atoms, where each carbon atom is at 120° angles with other neighboring carbon atoms. Moreover, the bond length between the carbons is 1.42 Å. Graphene exhibits a remarkably high surface area of 2630 m^2 g^{-1} and has unique optical properties (~2.3% adsorption of visible light), zero bandgap, high Young's modulus (1 TPa), an extremely high electron mobility of 200 000 (cm^2 V^{-1} s^{-1}), and it is up to two hundred times

ᵃFaculty of Materials Engineering, Sahand University of Technology, Tabriz, Iran. E-mail: nasirpouri@sut.ac.ir; f_nasirpouri@yahoo.com; Fax: +98 41 33444333; Tel: +98 41 33459450

ᵇDepartment of Inorganic Chemistry, Faculty of Chemistry, University of Tabriz, Tabriz, Iran

† Electronic supplementary information (ESI) available: The comparison between the most efficient coating in this research and the others reported in the literature which are mentioned in the introduction section. XRD patterns of GO and PGO, and EDX spectra of GO and PGO.. See DOI: 10.1039/d0ra10665h

stronger than steel. Graphene materials with different numbers of layers have found widespread usage in various fields, such as in electronic devices,[14–16] sensors and biosensors, carbon fibers in airplanes, strong plastics, and coatings.[17–20]

Graphene oxide (GO) is a common derivative of graphene with a compact structure, prepared *via* the oxidation of graphite.[21] GO sheets are covered by oxygenated species such as epoxide, alcohol, hydroxyl, carboxylic acid groups.[22] Thus, they can be dispersed very quickly in liquid media, such as water and organic solvents, using ultrasonic methods.[23] The functionalisation of GO sheets is an ideal method for their stabilization in different chemical environments. The attached compounds restrict the aggregation of GO sheets. Therefore, chemical or physical methods are used to tailor the functionalisation of GO. The functionalisation of GO has generally been conducted *via* three methods, including using chemical compounds, macromolecules, and nanoparticles. Organic compounds attach to the surface of GO by linking to the graphene sheets through "π" groups. The presence of hydroxyl and carboxyl groups helps to disperse the GO in water. In contrast, the existence of hydroxyl groups on the surface of GO is not very useful in organic techniques that use organic compounds, where functionalisation helps the GO to disperse in organic media.[24,25]

There have been several attempts to incorporate GO during the preparation of PANI to produce nanocomposites. Oxygenated functional groups with hydrophilic properties are generally used as precursors for synthesizing PANI composites. Self-assembly and *in situ* polymerization methods are well-known as methods for synthesizing PANI/GO nanocomposites.[26] Investigations using derivatives of PANI such as *p*-phenylenediamine (PPDA) have shown it to be an attractive material because of its specific properties such as a ladder-like structure, good conductivity (6.3×10^{-6} S cm^{-1}), and electroactivity, among the aromatic diamine family. PPDA is mainly used in electrical storage devices such as batteries and supercapacitors due to its unique capability to prevent the restacking of graphene layers in the GO structure due to functionalisation[27,28]

Epoxy and its nanocomposites are used in different fields such as in maritime, aerospace, and automobile applications, in sports equipment, buildings, electronic systems, and in anticorrosion coatings.[29] However, the widespread use of epoxy coatings is impeded because of their impaired abrasion and erosion of mechanical strength fracture and destruction. In addition, the presence of inherent holes in the epoxy facilitates the penetration of water into the coatings towards the substrate surface.[30] Studies have shown that making epoxy-based composites using different secondary phase materials such as conductive polymers, inorganic nanoparticles, and inorganic-conductive polymers improves the properties and performance of epoxy coatings.[31–37]

Conductive polymers such as PANI have a positive influence on the oxidation potential of a coating, which prevents the passive corrosion of the metal. Also, creating barriers between aggressive media and the substrate will be realized at the electrochemical interface created by polymers.[31–33] Moreover, inorganic materials added into the epoxy can resist the penetration of an aggressive environment and create zig-zag routes to diffuse corrosive species.[34–37] Composites composed of conductive polymers with nanoparticles like PANI–ZnO exhibit good properties such as anticorrosion and antifouling.[38–40] Recently, nanocomposites with graphene derivatives and conductive polymers have been reported to increase the quality of epoxy coatings.[41–43] In this field, we have recently demonstrated PANI–GO composites in epoxy coatings, which reveal a resistance of 2.70×10^6 Ω cm^2 for 12% GO after 192 h of immersion in brine, with suitable antifouling properties.[44] In such GO-modified polyaniline/epoxy coatings on low carbon steels, raising the concentration of GO in the paint does not slow down the corrosion rate because of the hydrophilicity of GO. However, some substances such as di-octyl phthalate and titanium dioxide grafted to GO improve the paint quality.[45] Shang *et al.* investigated the anti-corrosion behavior of a PGO/PANI nanocomposite as a secondary phase or pigment in polystyrene-matrix coatings. They found that PGO/PANI in the polystyrene-based materials exhibited a minimum corrosion rate of 1.68×10^{-4} mm per year, which is better than the performances of the individual PGO or PANI additives with polystyrene.[46] Recently, Wang *et al.* reported relatively similar work to our study, but with substantial differences. They investigated only the anticorrosion properties of the epoxy coating with the synthesized composites composed of functionalised GO with PPDA called GON having solely a mass ratio of PPDA to GO of 10, which was subsequently used *in situ* polymerization with different amounts of aniline (An) to produce GON–An nanocomposites. A constant ratio of the oxidizing agent $(NH_4)_2S_2O_8$ to An of 2.4 was used, while different GON–An nanocomposite mixtures with the same amount of GON and different amounts of An were demonstrated. It was shown that the GON–An02 composite raised the impedance of the epoxy coating from 6.3×10^8 Ω cm^2 to 1.9×10^{10} Ω cm^2 at the initial stage of immersion and 4×10^9 Ω cm^2 after 35 days of immersion in brine. However, it was shown that increasing the amount of aniline did not improve the resistance of the material against corrosion.[47] A comparison between the most efficient coating in this research and the other reported results is summarized in Table S1.† Our results not only detail the dual-functionality of epoxy-based coatings, of both anti-corrosion and anti-fouling properties, but we also aimed to investigate the effects of other synthesis parameters, such as changing the ratio of PPDA to GO, changing the loading of functionalised GO, the synthesis method, and the type of epoxy with lower resistance that provided better functional properties.

The primary purpose of this work was to produce more efficient GO–PANI composite pigments to be added to epoxy coatings. The synthesis of GO was performed using a mixture of oxidants including $(NH_4)_2S_2O_8$, which enhances the number of hydroxyl groups on the GO sheets. These groups allow some good connections to be made between GO and *p*-phenylenediamine. Chemically synthesized GO functionalised with *p*-phenylenediamine (PPDA) is referred to as PGO in this study. The functionalisation of GO was carried out in the absence of other organic compounds as well as with the elimination of N$_2$ gas blown in the reaction. This reaction was simply performed in deionized water at room temperature. PPDA, an organic

compound with the formula $C_6H_8N_2$, was used for the functionalisation and reduction of GO in this project. Using PPDA in the course of the synthesis of the composite led to good factors being exhibited, such as the elimination of the curling and crumpling of GO. The restacking of sheets occurred if the functionalised GO was dried after centrifuging and washing with deionized water. Thus, we kept the synthesized PGO in the *in situ* polymerization with aniline to reduce this. The time of reaction was therefore shortened by employing the above procedure. Furthermore, PPDA functionalised GO was used as a template for synthesizing PANI chains. In addition, PANI–PGO was produced by adding PANI targeted oxidation agents *via* an *in situ* polymerization method. So, the morphology of the composites was completely different from that of individual polyaniline. In this study, the PANI/PGO composite was introduced as a novel nanocomposite pigment in the epoxy-based coatings to investigate how increasing the amount of PGO in the structure of the composites led to efficient anti-corrosion and anti-fouling properties. The main products were useful pigments for the epoxy binder. The resistance of epoxy used in our project was inadequate against corrosion. In contrast, using the synthesized nanocomposites in epoxy materials improves the properties of the bare epoxy. The coatings were applied to the samples using a simple method as is generally used in industry. The optimized composition of the PANI–PGO nanocomposites achieved in this study will be an efficient alternative pigment for anti-corrosion and anti-fouling epoxy-based paint coatings for marine and related applications.

Experimental

Materials and instruments

Natural graphite, sodium nitrate ($NaNO_3$) from Merck (6535), potassium permanganate ($KMnO_4$) from Merck (105080), sulfuric acid (H_2SO_4, 98%) from Merck (100713), hydrogen peroxide (H_2O_2, 35%) from Merck, ethanol (C_2H_5OH 99.5%), hydrochloric acid (HCl, 35.4%) from Royalex-H125, aniline from Merck (822256), 1,4-phenylendiamine from Merck (8.07246.0250), ammonium persulfate (APS) from Merck (1.01209), NAYA epoxy resin (NPEL-127), ACR hardener (H3895), NaCl from Fluka AG-218541280, and deionized water were used in the experiments.

Synthesizing graphene oxide

0.5 g of graphite and 0.25 g of $NaNO_3$ were placed into a 500 mL round-bottom flask, to which 13 mL of H_2SO_4 was subsequently added. The mixture was left in an ice bath for 1 h until a viscous solution formed. Then, 1.5 g of $KMnO_4$ and 4.5 g of $(NH_4)_2S_2O_8$ (1 : 3) were added slowly to the viscous solution. During the addition of $KMnO_4$ and $(NH_4)_2S_2O_8$, the temperature was controlled and kept under 20 °C. The solution was removed from the ice bath after the addition of $KMnO_4$ was finished. The solution was stirred at room temperature for 24 h. Subsequently, 35 mL of deionized water was added very slowly to the solution, which was then heated up to 98 °C. In this step, golden pieces were observable in the solution. 5.5 mL of 35% vol H_2O_2

was added to the solution. At this stage, the temperature of the solution was reduced to avoid any risk of exothermic reactions involving H_2O_2. 20 mL of 10% vol HCl was added to eliminate any metal ions. Subsequently, 30 mL of deionized water was added to the solution. The mixing process was continued until the bubbles were removed. Finally, the solution was washed and centrifuged with deionized water. This process was continued until the pH reached 7. The centrifuged solution was dried off in an oven at 60 °C.[44,48]

Functionalisation and reduction of GO with PPDA

The diamine solution was prepared by dissolving *p*-phenylenediamine in deionized water. The produced solution was heated to 30 °C so that the dissolution of PPDA was completed. The mass ratio (GO/PPDA) was assumed to be 1 : 1.[49] The GO was dissolved in 25 mL of deionized water and immersed in an ultrasonic bath for 1 h. Then, the obtained solutions of diamine and GO were admixed. The mentioned mixture was heated to 80 °C for 30 min. Afterwards, it was washed *via* centrifuging in deionized water until the color of the rinsed water changed from purple to colorless. The utilisation of this procedure can be assumed to be an effective method for the removal of PPDA, which does not interact with the surface of GO. Subsequently, the mixture was heated at 30–40 °C in order to obtain a concentrate of 25 mL in volume. The obtained functionalised GO was named PGO (x), where x refers to the amounts of PPDA and PGO. For example, 0.05 g of PPDA–0.05 g of GO was named PGO (0.05), 0.1 g of PPDA–0.1 g of GO was named PGO (0.1), 0.2 g of PPDA–0.2 g of GO was named PGO (0.2), and 0.4 g of PPDA–0.4 g of GO was named PGO (0.4).
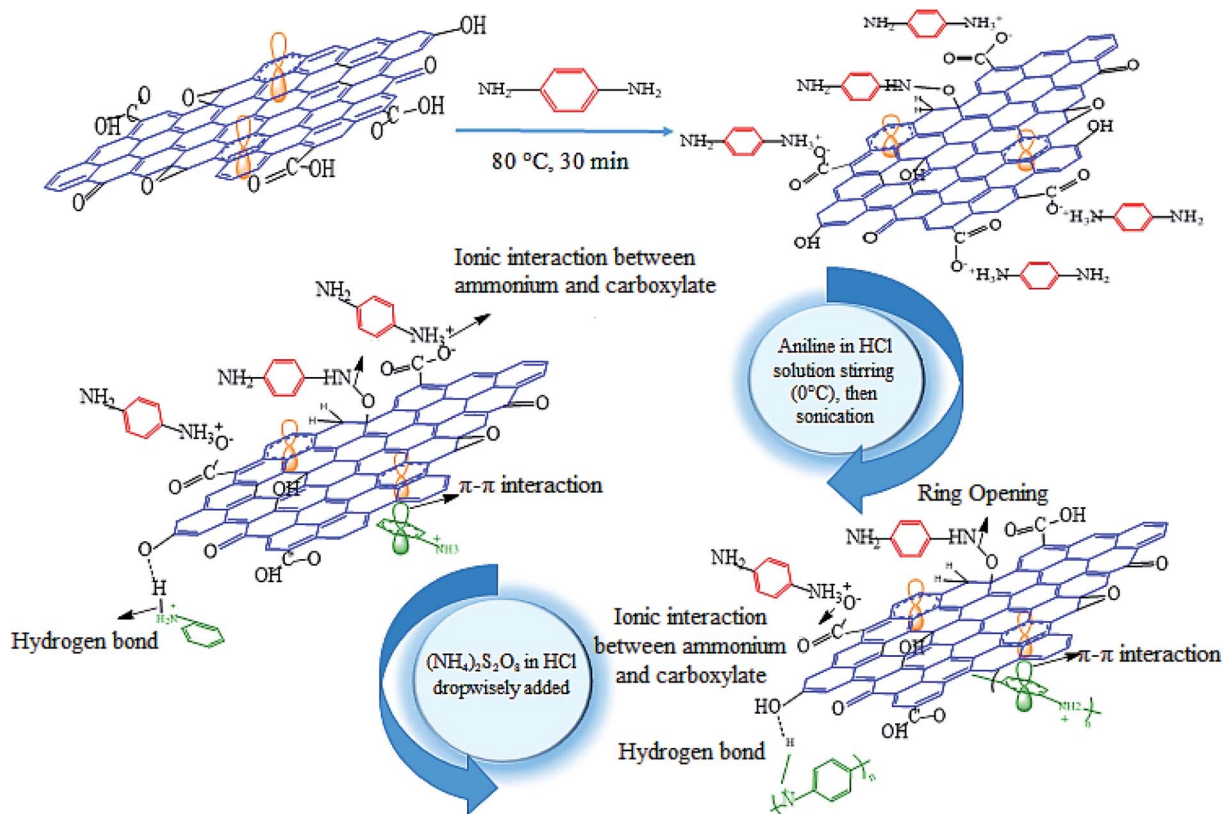
Synthesizing PANI–PGO nanocomposites

25 mL of different samples of functionalised GO (namely PGO) were sonicated for 1 h. A solution of 100 mL of HCl (1 M) and 2 mL of aniline was prepared and mixed with the different PGO solutions in an ice bath for 30 min. The obtained mixtures were sonicated in an ice bath for 1 h to achieve the complete dispersion of the aniline species between PGO papers. Then, a solution of 100 mL of 1 M HCl containing 4.8 g of $(NH_4)_2S_2O_8$ was added dropwise into the mixtures in an ice/water bath and magnetically stirred. *In situ* polymerization was then conducted at a low temperature (0 °C) for 3 h. The mixtures were sonicated in an ice bath for 2 h in order to minimize the aggregation of polymers and terminate the polymerization. The obtained precipitates were filtered and washed with ethanol and deionized water. The products were washed until the rinsed water became colorless. The prepared composites were dried at 60 °C under vacuum condition for 5 h.[44] The same procedure was used for synthesizing PANI. The procedure for synthesizing the PGO and PANI/PGO nanocomposites is shown in Scheme 1.

Preparation of the PANI–PGO nanocomposite coatings

Carbon steel (grade st-37) substrates with the dimensions 1 cm × 1 cm × 0.2 cm were prepared by polishing using sandpapers grades 80 up to 2000. Next, the polished steel substrates were

Scheme 1 Synthesis stages of PGO and the PANI–PGO nanocomposites.

cleaned by immersing them in ethanol solution with the assistance of an ultrasonic bath. An epoxy blend composed of 2 wt% PANI–PGO (x) composites was prepared. The blend was prepared by mixing epoxy with the composites at a stirring speed of 300 rpm for the first 30 min.[42,43,50] The epoxy blend was then further mixed for 45 min by sonicating it under 305 W at a frequency of 50/60 Hz to obtain homogenous and uniform epoxy paint with various PANI/PGO (x) nanocomposites. The sonication facilitated the dispersion of the nanocomposites in the epoxy emulsion and removed the bubbles produced during the magnetic stirring. Next, the hardener was dispersed into the mixture in a weight ratio of 1 : 2 (1: hardener (H-3895), 2: epoxy (NPEL-127)) and very slowly blended. The epoxy-matrix paint was applied using a brush. The paint coating was applied to the substrates before it became viscous. Subsequently, the samples were left for 24 h to dry at room temperature. The coating thickness, *i.e.* 200 ± 15 μm, was chosen to fulfill the requirements of marine coatings for wide applications.[39] The coatings were named E/PANI–PGO (0.05), E/PANI–PGO (0.1), E/PANI–PGO (0.2), and E/PANI–PGO (0.4).

Microstructural and compositional characterization of the epoxy-based coatings

The chemical bonding that took place during the synthesis was characterized using a Bruker Tensor 27 Fourier-transform infrared (FTIR) spectrometer employing the KBr pellet method. A MIRA TESCANE scanning electron microscope operating at 15 kV was used for taking field-emission scanning electron microscopy (FESEM) images. A Bruker D8 Advance AXS diffractometer equipped with a Cu K$_\alpha$ radiation source ($\lambda = 1.54$ Å) operated at 40 kV and 40 mA in the 2Θ range of 10–80° at a scan rate of 0.05 degrees per second was used to record the X-ray diffraction (XRD) patterns of the nanocomposites. The XRD pattern of PGO was characterized using a D500 Siemens diffractometer equipped with a Cu K$_\alpha$ radiation source ($\lambda = 0.154$ nm) over a 2Θ range of 4–70°.

Electrochemical testing of the corrosion behavior

The corrosion behavior of the epoxy coatings reinforced by the PANI/PGO (x) nanocomposites was investigated in 3.5% NaCl solution at room temperature using a conventional three-electrode test cell. An Autolab PGSTAT 30 instrument connected to the computer *via* an A/D interface was used to conduct the electrochemical tests. A platinum electrode and a standard Ag/AgCl electrode were chosen as the counter and reference electrodes, respectively. Electrochemical impedance spectroscopy (EIS) tests were performed under a perturbation voltage of 5 mV (rms) over the frequency range of 10 kHz to 100 mHz. The resulting data, including Nyquist and Bode plots, were obtained through the EIS tests. The data obtained were fitted using the ZView® (II) software to produce an equivalent electrical circuit and its parameters. Subsequently, the measurement of the thickness of the coatings was evaluated using an eXacto FN elcometer.

Antifouling properties of the E/PANI–PGO coatings

Carbon steel grade st-37 plates were used as the substrate for the investigation of the antifouling properties. The steel plates were cut with dimensions of 3×4 cm^2 and a thickness of 2 mm. The plates were painted with the epoxy-based PANI–PGO (x) paints, as described earlier. A simulated environment was prepared using a light-emitting diode (LED) lamp, oxygen pump, heater, and thermometer. The temperature was maintained in the range of 25–27 °C, adaptable conditions for plant growth, guppy fish, spirulina algae, and dwarf hair grass.

Results and discussion

FTIR study

The spectrum of GO confirms the existence of two types of (OH) groups, namely hydroxylic (OH) and phenolic (OH) groups. Thus, the use of $(NH_4)_2S_2O_8$ as a strong oxidant in the procedure of synthesizing GO results in some specific characteristics, such as the dispersion of GO sheets in the deionized water because of phenolic OH. Therefore, the preparation of the GO composites becomes easier, as will be discussed later. The FTIR spectrum of GO demonstrates a wide peak in the range of 3000–3500 cm^{-1}. The (–C=O) stretching vibration appears in the 1745 cm^{-1} region.[51,52] The peak occurring in the 1577 cm^{-1} is related to (C=C) bonding.[52] Peaks for (C–O) in the carboxylic (C–OOH) and epoxy (C–O) vibrations are observed at 1403.75 and 1075 cm^{-1}, respectively.[53] The broad peak seen at 690 cm^{-1} corresponds to (C–H) bonding. The FTIR spectrum of GO has more (OH) groups than other functional groups. Glukhavan and co-workers' theoretical investigations justified this phenomenon. They found that the barrier activation energy for groups such as epoxy is more than that of the hydroxyl groups. As a result, the (OH) groups attach to the surface easier than the epoxy groups. Also, Glukhavan *et al.* concentrated on the number of graphene sheets, *i.e.*, one and two-layer graphene in the course of the oxidation in their theoretical investigation,[54] and the activation energy was measured. They found that increasing the number of graphene sheets decreases the activation energy for functionalisation. In contrast, the bonding energy and enthalpy of the reaction increase. This study showed clearly that two-layer graphene is functionalised easier than its one-layer counterpart. Nevertheless, separating the functional groups from two-layer graphene is harder. Therefore, the graphite sheets connected *via* van der Waals forces have more opportunity to oxidize under the oxidation conditions of the preparation. The FTIR spectrum of GO is shown in Fig. 1a.

The FTIR spectra of GO, PPDA, and PGO show that some of the peaks are omitted, covered, or have shifted to higher wavenumbers when their spectra are compared with each other, which can be observed in Fig. 1a, b, and c, respectively. The addition of PPDA to the GO suspension in the deionized water has some effects on the FTIR spectrum of the GO. The peak for the (NH–) of the PPDA appears in the range of 3195–3300 cm^{-1}, and is displaced after adding the GO to the PPDA mixture. Therefore, the NH-peak shifts to a higher wavelength of 3700 cm^{-1}. Then, the intensity of some peaks, such as those of
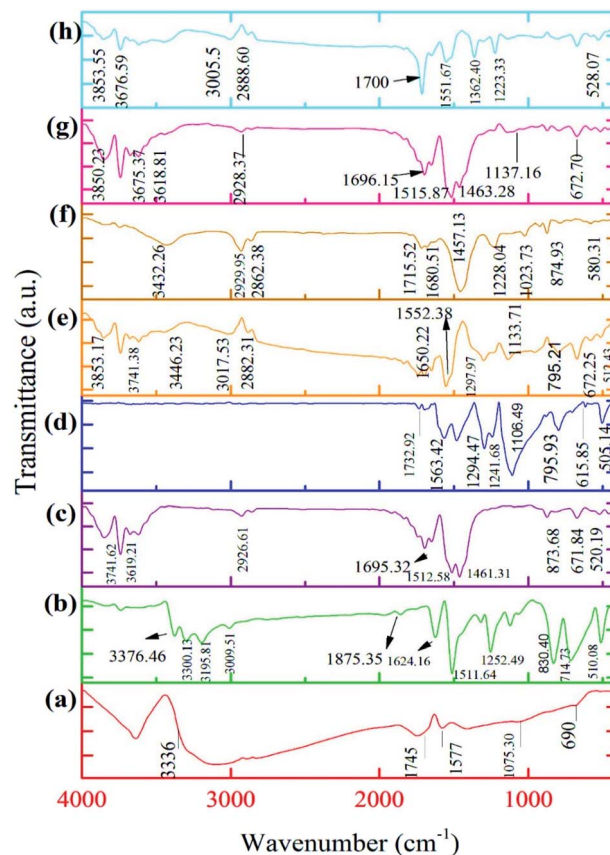

Fig. 1 FTIR spectra of (a) GO, (b) PPDA, (c) PGO, (d) PANI, (e) PANI–PGO (0.05), (f) PANI–PGO (0.1), (g) PANI–PGO (0.2), and (h) PANI–PGO (0.4).

the epoxy and hydroxyl groups, is related to the GO and is decreased by using PPDA for functionalisation. The reduction in the intensity of the epoxy group peak at 1226 cm^{-1} can be attributed to the interaction of a diamine with epoxy groups *via* a ring-opening reaction. Moreover, one vibration in the range of 2800–3000 cm^{-1} for PGO can be observed owing to =C–H bonding. This peak entirely proves the existence of aromatic diamines on the PGO surface. A stretching band at 1500 cm^{-1} is related to the C–N bonding in PGO; the mechanism of this process is an SN_2 nucleophilic substitution and ring-opening reaction between the carbon atoms in GO and nitrogen in diamine.[49] The stretching peaks at 3850 and 1100 cm^{-1} can be ascribed to N–H and C–N, respectively.[55–57] The peaks at 1649, 1512 and 824 cm^{-1} can be attributed to the N–H, C=C, and C–H, respectively, of a benzene ring with *para*-substitution.[58]

The FTIR spectrum of PANI is well-known to have peaks at 1106, 1249, 1480, and 1563 cm^{-1}.[59] The absorption peaks related to the benzene and quinone rings appear at 1480 and 1563 cm^{-1}, respectively. Synthesis of the PANI in its emeraldine form was proven from the intensity of the FTIR spectra peaks. As Fig. 1d shows, the benzene ring absorption peak is more intense than that of the quinone ring.[60] The stretching vibration outside and inside of the C–H molecular plane can be observed at 795 and 1127 cm^{-1}, respectively.[61] The stretching vibration of
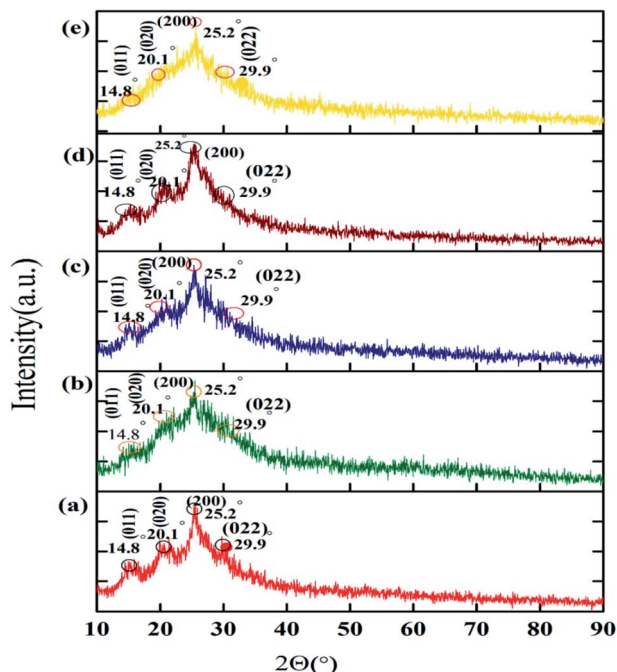
Fig. 2 XRD diffraction patterns of (a) PANI, (b) PANI–PGO (0.05), (c) PANI–PGO (0.1), (d) PANI–PGO (0.2), and (e) PANI–PGO (0.4).

Table 1 EDX analysis of PGO and GO

	Element	Wt%	At%
Functionalized graphene oxide (PGO)	C	61.64	66.47
	O	21.54	19.91
	N	16.83	13.62
Graphene oxide (GO)	C	45.74	52.9
	O	54.26	47.10

groups make the surface of PGO more electronegative than its bare form. Moreover, protonation of PANI takes place *via* an oxidation reaction, because of the presence of HCl in the course of the synthesis. Thus, the PANI becomes electropositive. Consequently, a homogenous combination is achieved due to the existing electrostatic interactions. The strong interactions between the PGO sheets and the PANI occur because the surface of PGO plays a perfect role as a template and is a suitable place for the nucleation of PANI.[59,62,63]

Peaks occurring at 1480 and 1563 cm^{-1} in the FTIR spectrum of the PANI were shifted by 5 to 15 cm^{-1} in the spectra of the nanocomposites. This shifting can be attributed to the π–π interactions between the quinoid and benzenoid rings of the PANI polymer chains and PGO sheets. This creates a greater π electron domain which blocks the movement of the functional groups in the nanocomposites.[46] The FTIR spectra of the synthesized nanocomposites are shown in Fig. 1.

–C–N and –C=N are related to the 1294 cm^{-1} and 1241 cm^{-1} peaks, respectively.[61] The peak at 1563 cm^{-1}, which exists in the spectrum of the pure form of PANI, shifts to higher wave-numbers after the synthesis of the composites, with a blue shift detected. The C–O, O–H, and other peaks are detected in the composite form, as we can see from their FTIR spectra, shown in Fig. 1e–h. These peaks correspond to the connection between the PANI chains and the PGO sheets. This relationship between the PGO and PANI is due to the electrostatic, hydrogen bonding, and π–π stacking interactions that arise as a result of the existence of PGO in the reaction medium. The electrostatic interactions are introduced by functionalised groups such as CHO, COOH, OH, and epoxy on the surface of the PGO. These

XRD analysis

A sharp peak for GO is present in its pattern at $2\Theta = 11.57°$, as shown in Fig. S1.† Moreover, this peak is observed after adding oxidant agents, and after the graphite peak ($2\Theta = 26.5°$) in the XRD pattern was eliminated. The distance of the sheets increases from 0.35 to 0.77 nm after using Hummers' method to synthesize GO. This estimation was obtained using the Bragg equation, eqn (1):
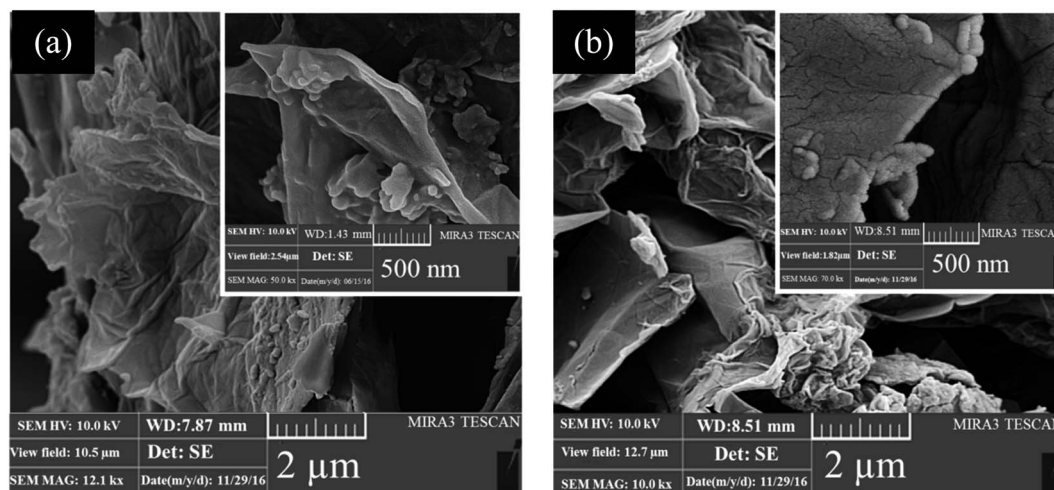
$$n\lambda = 2d \sin \Theta, \tag{1}$$

Fig. 3 FESEM images of (a) GO and (b) PGO.
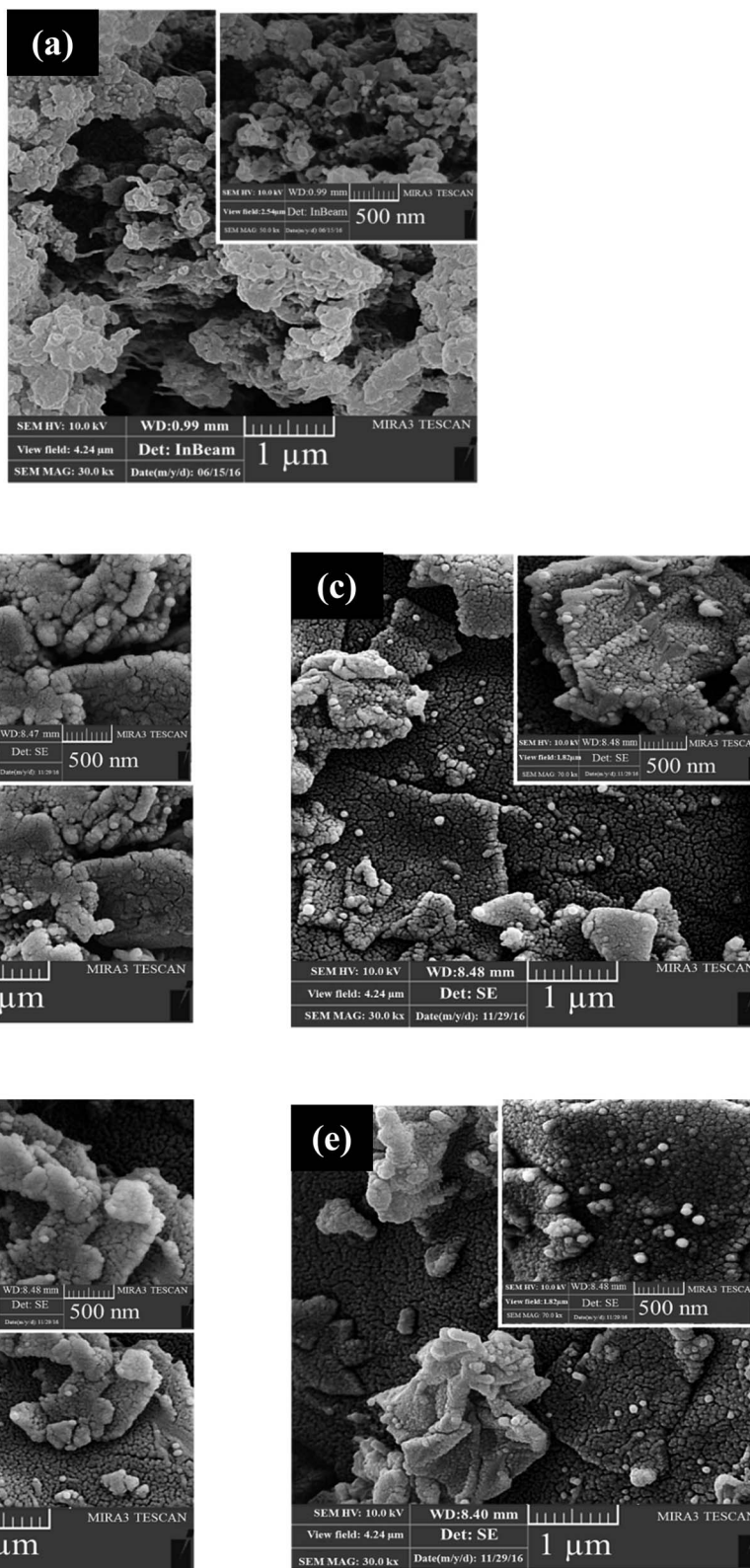
Fig. 4 FESEM images of (a) PANI, (b) PANI–PGO (0.05), (c) PANI–PGO (0.1), (d) PANI–PGO (0.2), and (e) PANI–PGO (0.4).

where λ is the X-ray wavelength of Cu K$_\alpha$ radiation (1.54 Å), d is the space between lattice planes, θ is the reflection angle and n is equal to 1.

The increase in the distance between the graphene sheets is related to the incorporation of –OH, C–OOH, C=O, and C–O functional groups in the GO structure.[64]
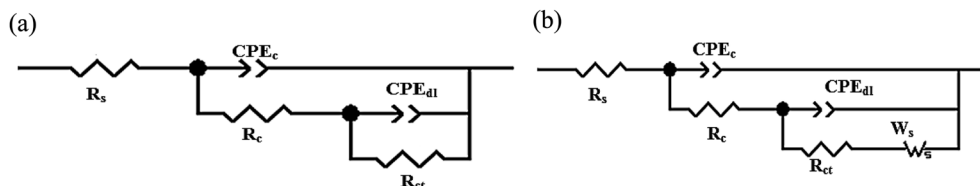
Fig. 5 Equivalent circuits used for (a) fitting all types of coating at various times and (b) fitting of E/PANI–PGO(0.05) after 2h.

After the functionalisation of GO, the peak occurring at 11.57° disappears, but three other diffraction peaks appeared. The first peak occurs at $2\Theta = 7.99°$, which proves that the PPDA polymer attached between the GO sheets, resulting in an increase in the distance between the GO sheets from 7.7 to 11.87 Å. The second peak, which can be seen at 24.7°, confirms that the GO sheets were partly reduced, and that the GO eventually lost most of its oxygen-containing functional groups. Subsequently, the distance between the sheets decreased from 7.7 to 3.6 Å. Moreover, the last peak was detected at around 43°, and

this peak proves that some of the graphene sheets agglomerated.[65]

The PANI shows good crystallinity, as we show in Fig. 2a. This crystallinity of PANI is related to the usage of HCl as the medium in its synthesis. The XRD patterns show some peaks at 9.5°, 14.8°, 20.1°, 25.2°, 26.8°, and 29.9° relating to the (001), (011), (020), (121), and (020) planes of PANI, respectively.[59]

As Fig. 2 shows, the prominent peaks of PGO disappeared, and the PANI–PGO nanocomposites have the same XRD patterns as that of PANI. The prominent peak for PANI appears
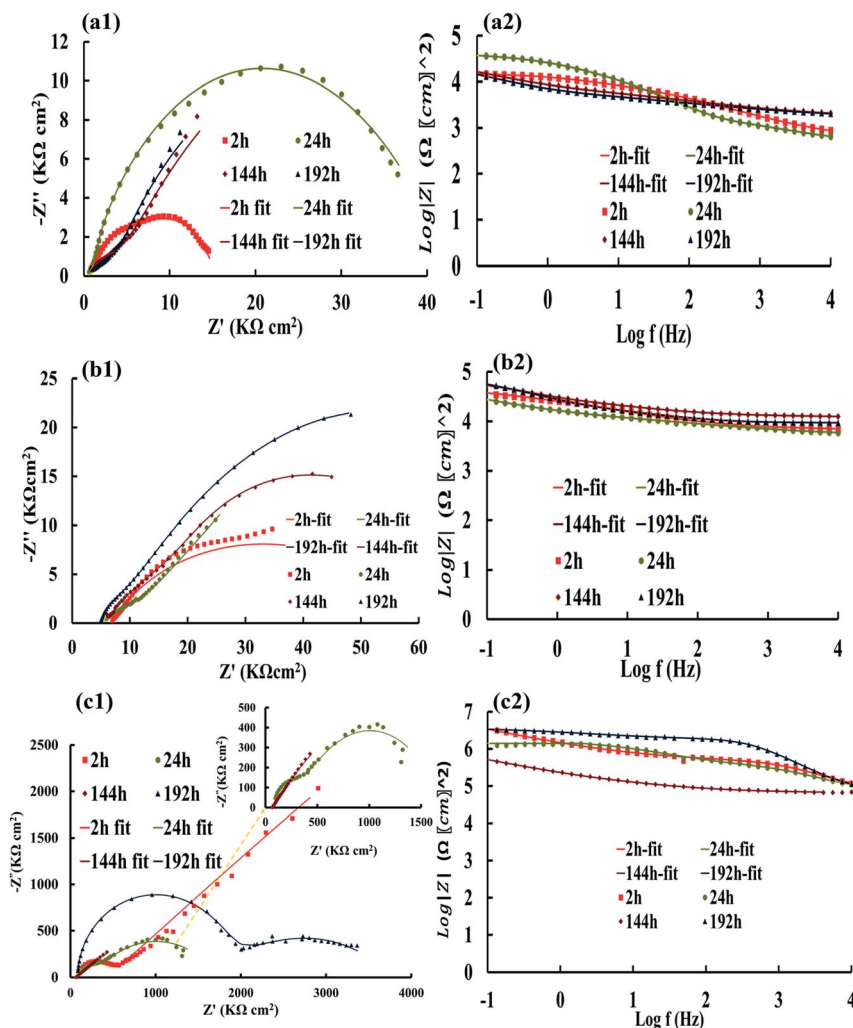

Fig. 6 (a1) Nyquist plot of the epoxy sample, (a2) Bode plot of the epoxy sample, (b1) Nyquist plot of the E/PANI sample, (b2) Bode plot of the E/PANI sample, (c1) Nyquist plot of the E/PANI–PGO (0.05) sample, and (c2) Bode plot of the E/PANI–PGO (0.05) sample EIS data after specific times.

at $2\Theta = 25°$ in all of the XRD patterns. PGO has the function of nucleating PANI chains onto it. The XRD patterns of the PANI–PGO nanocomposites prove the simultaneous presence of PGO and PANI in the materials.

FESEM measurements

As shown in Fig. 3a, the FESEM images of GO prove that it has a layered structure, with the thickness of the sheets measured to be around 45.78–53.83 nm. The EDX analysis shows that the percentage of oxygen and nitrogen is around 50 wt%, as reported in Table 1, and the EDX spectra of PGO and GO are shown in Fig. S2.†

The FESEM images demonstrate that the functionalised GO has a particular structure, which is different from that of the bare GO. SEM images of PGO are shown in Fig. 3b, which shows its well-known crumpled sheets.[25] The EDX analysis ultimately confirmed that reduction happens in the structure of the GO, as reported in Table 1. The percentage of the oxygen in the material decreased, but those of carbon and nitrogen increased.

FESEM images of the PANI and the nanocomposites are shown in Fig. 4. PANI has a spherical structure with an average grain size of 44–48 nm, which is agglomerated in some parts, as seen in Fig. 4a. PANI with a spherical structure attaches to the surface of PGO, the layered structure of which is clearly evident from the FESEM images even after adding more PGO to form the PANI–PGO nanocomposites. As is evident from the FTIR and XRD examinations, the functionalised graphene layers are separated from each other at a farther distance than the neat graphene sheets. PANI nanoparticles formed on the surface of the functionalised GO discourage the GO sheets from curling and crumpling, as is confirmed from FESEM images shown in Fig. 4.

Corrosion behavior of the E/PANI–PGO (*x*) coatings

Electrochemical impedance spectroscopy (EIS) studies. EIS measurements were carried out in order to investigate the corrosion behavior of our different materials, including pure epoxy, PANI, E/PANI–PGO (0.05), E/PANI–PGO (0.1), E/PANI–PGO (0.2), and E/PANI–PGO (0.4) coatings.
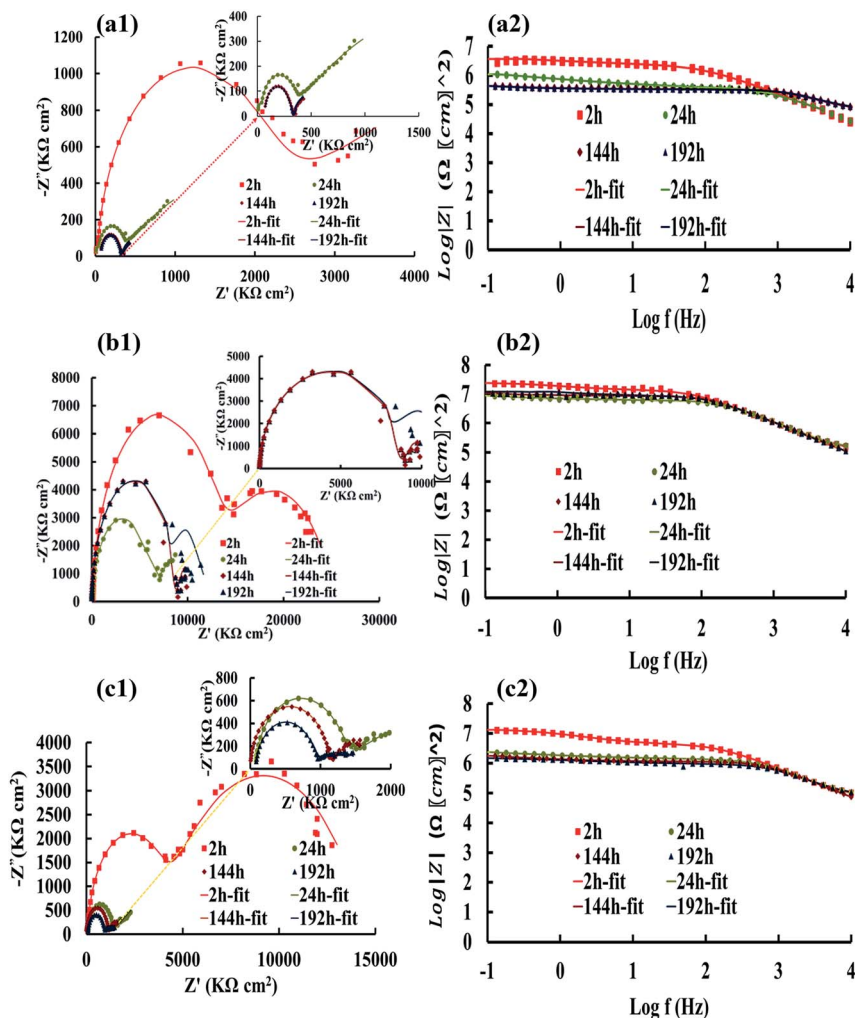

Fig. 7 (a1) Nyquist plot of the E/PANI–PGO (0.1) sample, (a2) Bode plot of the E/PANI–PGO (0.1) sample, (b1) Nyquist plot of the E/PANI–PGO (0.2) sample, (b2) Bode plot of the E/PANI–PGO (0.2) sample, (c1) Nyquist plot of the E/PANI–PGO (0.4) sample, and (c2) Bode plot of the E/PANI–PGO (0.4) sample EIS data after specific times.

Fig. 5 demonstrates the two equivalent circuits that fit the data points of the EIS data, which were measured using an Autolab instrument. In the EIS studies of the epoxy coatings, there are two loops in the equivalent circuits. These two capacitive loops, which are seen for epoxy coating, correspond to the organic coating in the high-frequency region and pores with defects in the low-frequency region.[66,67] The equivalent circuits consist of R_s, R_{ct}, R_c, CPE_{dl}, CPE_c, and the Warburg element, which represent the electrolyte resistance, the charge transfer resistance, the coating pore resistance, the constant phase element of the double-layer capacitance, the coating capacitance, and the Warburg impedance, respectively. The fitting with equivalent circuits proves that the R_s values are negligible compared with the R_c and R_{ct} values. The anticorrosion properties of epoxy matrix including (2 wt%) PANI–PGO nanocomposite were determined in 3.5% NaCl solution.[68]

The Nyquist and Bode plots of the different coatings in the 3.5% NaCl at specific intervals (after 2, 24, 144, and 192 h) are shown in Fig. 6 and 7. The data obtained from the fitted plots using the equivalent circuits are summarized in Table 2 for the various coatings. The simplest way of identifying the quality of the coatings against corrosion has been proposed by comparing the Bode plots of the coatings at low frequencies ($|Z|_{0.1Hz}$).[69,70] The resistance of the coatings generally decreases after a long immersion time because of open micropores inside the nanocomposite, which facilitate the penetration of electrolyte. This opens up diffusion paths for the electrolyte; however, we found that the PANI–PGO nanocomposites can block them. Thus, this protects the steel surface against the corrosive environment. Under any circumstances, when a negligible amount of electrolyte finds a way to reach the interface of the metal and coating, there is the possibility of the accumulation of corrosion products at the interface of steel/coating, which increases the resistance of imperfect quality coatings.[71] Furthermore, the impedance of coatings increased because the existing passive layer restricts the electrolyte from reaching the surface of the metal. The Bode plots completely proved that the PANI–PGO composites improve the quality of the epoxy coating. Also, the corrosion resistances extracted from the Bode plots at 0.1 Hz for the epoxy, E/PANI–PGO (0.05), E/PANI–PGO (0.1), E/PANI–PGO (0.2), and E/PANI–PGO (0.4) coatings are 1.47×10^4, 3.77×10^4, 3.41×10^6, 3.59×10^6, 2.39×10^7, 1.31×10^7 Ω cm² after 2 h immersion in brine water, respectively. In addition, the Bode plots of our different coatings at 0.1 Hz after one day of immersion show that E/PANI–PGO (0.2) has the highest quality amongst all of the coatings as this coating has a corrosion resistance 230.64 times higher than that of bare epoxy. Comparing our present results to a similar report by Wang *et al.*, it was shown that the best corrosion resistance achieved by their nanocomposite (GON–An02E) raised the corrosion resistance up to 30.15 times more than that of bare epoxy at 0.01 Hz after one day of immersion in brine,[47] which is far less than our reported value. This demonstrates the excellent anti-corrosion behavior of the nanocomposites prepared in this work.

Hence, the Bode plots shown in Fig. 6 and 7 confirm that the E/PANI–PGO (0.05), E/PANI–PGO (0.1), E/PANI–PGO (0.2), and E/PANI–PGO (0.4) nanocomposite coatings at low frequency

Table 2 Electrochemical data of the different coatings on steel in 3.5 wt% NaCl solution after fitting with equivalent circuits

Sample	R_c (Ω cm²)	CPE_c (nF cm⁻²)	R_{ct} (Ω cm²)	CPE_{dl} (nF cm⁻²)
Epoxy (E)				
2 h	1.01×10^4	4.87×10^{-6}	4.73×10^3	2.8×10^{-5}
24 h	2.13×10^3	6.87×10^{-6}	4.03×10^4	2.44×10^{-7}
144 h	9.90×10^3	3.49×10^{-5}	2.10×10^4	4.81×10^{-5}
192 h	1.00×10^4	5.77×10^{-5}	2.49×10^4	5.21×10^{-5}
PANI				
2 h	9.29×10^3	6.75×10^{-6}	5.04×10^4	2.11×10^{-5}
24 h	1.67×10^4	1.44×10^{-5}	3.83×10^4	3.828×10^{-5}
144 h	3.49×10^4	1.34×10^{-5}	3.84×10^4	9.15×10^{-6}
192 h	6.82×10^3	2.79×10^{-6}	8.70×10^4	1.63×10^{-5}

Sample	R_c (Ω cm²)	CPE_c (nF cm⁻²)	R_{ct} (Ω cm²)	CPE_{dl} (nF cm⁻²)	W (Ω^{-1} s^n cm⁻²)
E/PANI–PGO (0.05)					
2 h	3.69×10^5	7.01×10^{-10}	5.63×10^6	4.01×10^{-7}	4.91×10^8
24 h	3.03×10^5	1.60×10^{-9}	1.33×10^6	6.46×10^{-7}	—
144 h	1.86×10^5	1.37×10^{-9}	2.00×10^6	1.24×10^{-6}	—
192 h	1.72×10^6	2.41×10^{-10}	1.95×10^6	2.00×10^{-7}	—
E/PANI–PGO (0.1)					
2 h	1.89×10^6	1.10×10^{-10}	6.60×10^6	3.71×10^{-7}	
24 h	2.83×10^5	5.97×10^{-10}	2.51×10^6	1.00×10^{-6}	
144 h	2.61×10^5	6.32×10^{-10}	5.87×10^5	8.63×10^{-6}	
192 h	2.57×10^5	5.90×10^{-10}	9.08×10^5	8.88×10^{-6}	
E/PANI–PGO (0.2)					
2 h	1.34×10^7	1.58×10^{-10}	1.17×10^7	2.76×10^{-8}	
24 h	5.99×10^6	1.61×10^{-10}	6.39×10^6	2.69×10^{-7}	
144 h	8.78×10^6	1.60×10^{-10}	2.05×10^6	3.55×10^{-7}	
192 h	8.87×10^6	1.68×10^{-10}	2.60×10^6	3.50×10^{-7}	
E/PANI–PGO (0.4)					
2 h	4.22×10^6	2.30×10^{-10}	1.01×10^7	2.88×10^{-8}	
24 h	1.19×10^6	2.61×10^{-10}	2.00×10^6	7.15×10^{-7}	
144 h	1.12×10^6	2.59×10^{-10}	8.00×10^5	8.11×10^{-7}	
192 h	8.13×10^5	2.72×10^{-10}	7.58×10^5	6.10×10^{-7}	

($|Z|_{0.1Hz}$) are excellent at protecting against corrosion. In contrast, the E/PANI and epoxy coatings showed the worst performance. The coatings reinforced with PANI/PGO nanocomposites with PGO (0.2) and PGO (0.4) show remarkably better properties than the other nanocomposite coatings. By analyzing the EIS data, it can be seen that the amount of PGO in the nanocomposites has a critical impact on the properties of the coatings. The anticorrosion quality of the coatings is in the order of neat epoxy < E/PANI < E/PANI–PGO (0.05) < E/PANI–PGO (0.1) < E/PANI–PGO (0.4) < E/PANI–PGO (0.2). As displayed in Fig. 6(c1) and (c2), the Warburg element appeared only after 2 h in the data for the E/PANI–PGO (0.05) coating at low frequency.

The Warburg element's main role in the E/PANI–PGO coating is related to the restriction of the diffusion corrosive species. So, the EIS data of the E/PANI–PGO coating can be fitted to the equivalent circuit in Fig. 5b.[68,72] In other words, the magnitude of the Warburg resistance shows the good ability of
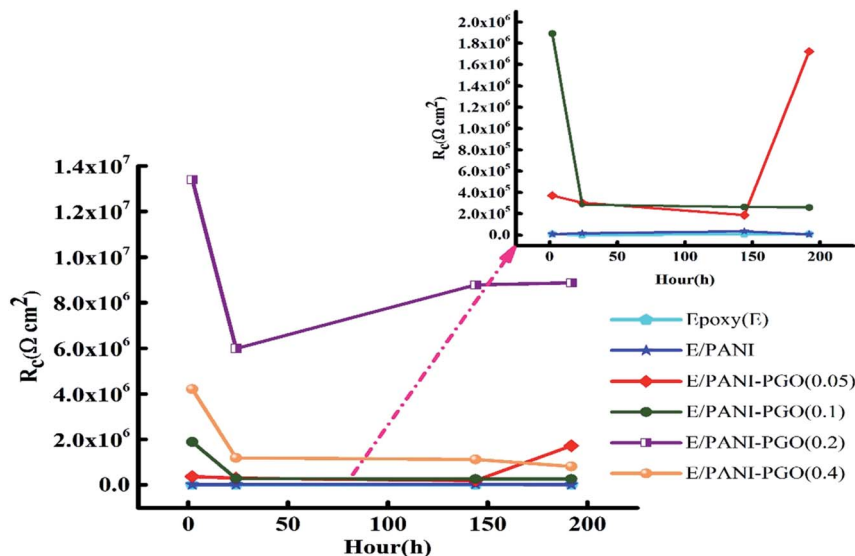
Fig. 8 The R_c values of the six coatings at different time intervals.

the PANI–PGO (0.05) nanocomposite blended into the epoxy in increasing the protection of the metal surface from corrosive electrolyte. The amount of PGO in the structure of the PANI–PGO nanocomposites plays a significant role in promoting and improving the quality of the epoxy matrix coatings against corrosive environments. The dispersion and exfoliation qualities of the nanocomposites in the epoxy matrix influence the barrier properties of the epoxy coatings. The coating with a large amount of PGO (0.4) (E/PANI–PGO (0.4)) compared with E/PANI–PGO (0.2) did not show good properties for prevention of corrosion. This fact was corroborated by the low dispersion quality of PANI–PGO (0.4) in occupying micropores.

We used some factors to interpret the anticorrosion properties of the PANI–PGO nanocomposites in the epoxy matrix. The presence of PPDA in the structure of GO limits the aggregation of PANI and makes it more smoothly disperse in the composite. A comparison between the PANI and PANI/PGO composite coatings shows that the PANI/PGO composite coatings are very well dispersed in the epoxy matrix compared with bare PANI. Filling the micropores of the epoxy matrix can restrict and change the direction of the corrosive electrolyte. Therefore, the penetration of electrolyte or diffusion paths will be zig-zag rather than straight when the micropores are filled by the nanocomposite. The active coatings prepared by the PANI–PGO nanocomposites can protect the surface from the corrosion environment. Also, they resist the diffusion of corrosive ions (Cl⁻) because of the negative surface charge created by the PANI–PGO in the epoxy matrix.[73,74]

Resistance and capacitance of the coatings as a function of the immersion time

Fig. 8 demonstrates the resistance of the different coatings against corrosion in 3.5 wt% NaCl solution based on the EIS tests. In general, the E/PANI–PGO (0.2) and E/PANI–PGO (0.4) coatings were more corrosion resistant than the other

coatings. The coating resistance decreased after increasing the PGO loading in the composite up to 0.4 g. Fig. 8 shows the resistance of the coatings at different time intervals. We can observe that there are two different anticorrosion performances as a function of the immersion time. First, the coating resistance decreases with an increase in the immersion time in 3.5% NaCl electrolyte. The rest of the oxygen groups that exist in the structure of the PGO sheets make the nanocomposite slightly hydrophilic. The absorption of water is one of the reasons that affects the decreasing behavior of the anticorrosion properties of the coatings during their immersion in brine. In contrast, this decrease has less impact on the quality of the epoxy coating reinforced with nanocomposite when compared with bare epoxy or the E/PANI coating. Also, low resistance coatings such as neat epoxy and E/PANI show increased anti-corrosion behavior after 24 h. E/PANI–PGO (0.05) shows an increase in anti-corrosion behavior after 144 h. This boost can be confirmed by the accumulation of a passive layer at the interface of metal/coating that occurs as a result of the diffusion of electrolyte. This passive layer has a positive effect on protecting the surface from further corrosion or delays this procedure.

Capacitance is a useful element in equivalent circuits for measuring electrolyte diffusion. The CPE values of epoxy coatings during the investigations are summarized in Table 2. The diffusion of electrolyte in the epoxy coating could be confirmed by CPE_c values duration immersion in 3.5 wt% NaCl. Furthermore, these evaluations proved the decayed quality of the epoxy coating with increased immersion time. The diffusion of the electrolyte into the interface of the metal/coating is associated with some issues, such as the blistering and swelling of the coatings at specific points. Having compared the CPE_c values listed in Table 2, we found that E/PANI–PGO (0.2) and E/PANI–PGO (0.4) have the lowest CPE_c values amongst the coatings investigated in this study.

The CPE_c value of E/PANI–PGO (0.05) after 2 h was lower than after two other time intervals (24 and 144 h). Therefore, the
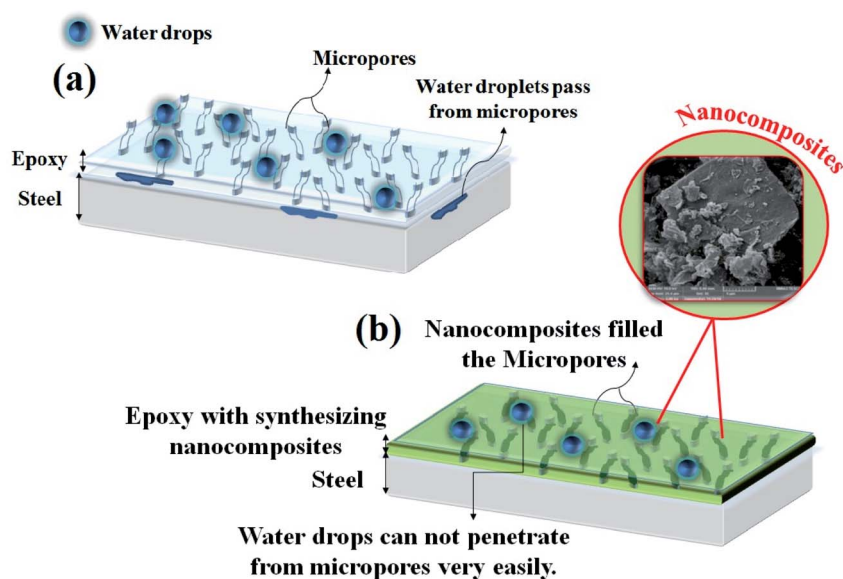
Fig. 9 The E/PANI–PGO coating performance after time connected to a corrosive electrolyte.

Warburg element in the EIS measurements of E/PANI–PGO (0.05) was verified after 2 h. This element disappears in the other Nyquist plots of the E/PANI–PGO (0.05) coating after longer periods of immersion. CPE_{dl} is a parameter for comparing the adhesive force in the wet situation. The lowest CPE_{dl} value was observed for the E/PANI–PGO (0.2) coating amongst the other synthesized coatings.

Anticorrosion properties of the E/PANI–PGO coatings

Fig. 9 graphically shows the capability of the PANI–PGO nanocomposite coatings for their use in developing high quality epoxy paints against corrosive environments. As shown in Fig. 9a, the pure epoxy coating has lots of holes and is colorless. These micropores allow droplets to reach the interface metal/coating. In

Fig. 9b, the reinforced coating with the PANI–PGO nanocomposite can be seen to confine the diffusion paths of corrosive electrolyte towards the surface of the metal. The application of the PANI–PGO nanocomposite in the epoxy matrix changes its color from colorless to green. Furthermore, the PANI on the PGO sheets fills the micropores and makes zig-zag routes that prolong the time it takes for electrolyte droplets to reach the surface.

Antifouling properties of the E/PANI–PGO coatings

The antifouling performance of the E/PANI–PGO coatings was studied under simulated conditions similar to those of a marine environment. The prepared aquarium was composed of the materials prepared in this work and included guppy fish, spirulina algae, and dwarf hair grass. After three months of immersion, the

Fig. 10 The E/PANI–PGO coatings before and after their immersion in an aquarium environment for three months.

© 2021 The Author(s). Published by the Royal Society of Chemistry

surfaces of the coated steel substrates were investigated at the macroscopic level. The neat epoxy coating sample was still colorless before the test, but turned green as a result of the accumulation of fouling pollutants. In addition, corrosion products such as rust were observed at the interface of the metal/coating. The color of the PANI coating changed from dark green to pale green, which proves the failure of the PANI coating, and the conditions that allow fouling are facilitated because of the exchange of lots of ions. As shown in Fig. 10, we observed that the E/PANI–PGO (0.05) and E/PANI–PGO (0.4) coatings show low stability against fouling. Despite this, the E/PANI–PGO (0.1), and E/PANI–PGO (0.2) coatings show good stability against fouling.

Conclusion

GO was successfully synthesized using the modified Hummers' method and functionalised using p-phenylenediamine, which was named PGO in the absence of any organic compounds and injection of any N_2 gas. PGO in suspension form was directly used in the synthesis of the PANI–PGO nanocomposites in order to prevent the stacking of the sheets. In this study, the anticorrosion and antifouling properties of commercialized epoxy coatings were substantially improved by adding PANI–PGO composites, since the latter fill the micropores of the epoxy. The loading of PGO in the nanocomposites influenced the quality of the epoxy coatings, with E/PANI–PGO (0.2) and E/PANI–PGO (0.4) showing the best anticorrosion performance. The E/PANI–PGO (0.4) coating is less resistive against corrosion than the E/PANI–PGO (0.2) coating. This corresponds to the low dispersion ability of the PANI–PGO (0.4) nanocomposites in the epoxy matrix due to their agglomeration, which occurred during their synthesis. This agglomeration leads to a lower filling of the epoxy micropores by PANI-PGO (0.4) than PANI/PGO (0.2). E/PANI–PGO (0.2) showed a performance 5.15 times higher than that of E/PANI–PGO (0.05) after long-term immersion (192 h) in 3.5 wt% NaCl solution. Comparison of the EIS data shows that E/PANI–PGO (0.2) coating exhibits the best resistance against corrosion. A simulated environment was employed to examine the antifouling properties at the macroscopic level, with E/PANI–PGO (0.1) and E/PANI–PGO (0.2) showing the best antifouling properties after three months.

Conflicts of interest

There are no conflicts to declare.

Acknowledgements

References

1 G. H. Koch, M. P. Brongers, N. G. Thompson, Y. P. Virmani and J. H. Payer, *Corrosion cost and preventive strategies in the United States*, Federal Highway Administration, United States, 2002.

2 J. E. Ramón, J. M. Gandía-Romero, M. Valcuende and R. Bataller, Integrated sensor network for monitoring steel corrosion in concrete structures, *VITRUVIO-International Journal of Architectural Technology and Sustainability*, 2016, **1**(1), 65–79.

3 S. Böhm, Graphene against corrosion, *Nat. Nanotechnol.*, 2014, **9**(10), 741–742.

4 R. J. Rathish, R. Dorothy, R. Joany and M. Pandiarajan, Corrosion resistance of nanoparticle-incorporated nano coatings, *Eur. Chem. Bull.*, 2013, **2**(12), 965–970.

5 I. Zvonkina and M. Soucek, Inorganic–organic hybrid coatings: common and new approaches, *Curr. Opin. Chem. Eng.*, 2016, **11**, 123–127.

6 M. Montemor, Functional and smart coatings for corrosion protection: a review of recent advances, *Surf. Coat. Technol.*, 2014, **258**, 17–37.

7 M. J. Nine, M. A. Cole, D. N. Tran and D. Losic, Graphene: a multipurpose material for protective coatings, *J. Mater. Chem. A*, 2015, **3**(24), 12580–12602.

8 A. G. Nurioglu and A. C. C. Esteves, Non-toxic, non-biocide-release antifouling coatings based on molecular structure design for marine applications, *J. Mater. Chem. B*, 2015, **3**(32), 6547–6570.

9 C. Hellio and D. Yebra, *Advances in marine antifouling coatings and technologies*, Elsevier, 2009.

10 P. A. Sørensen, S. Kiil, K. Dam-Johansen and C. E. Weinell, Anticorrosive coatings: a review, *J. Coat. Technol. Res.*, 2009, **6**(2), 135–176.

11 C. Ning, L. Mingyan and Z. Weidong, Fouling and corrosion properties of SiO_2 coatings on copper in geothermal water, *Ind. Eng. Chem. Res.*, 2012, **51**(17), 6001–6017.

12 A. Rosenhahn, T. Ederth and M. E. Pettitt, Advanced nanostructures for the control of biofouling: the FP6 EU integrated project AMBIO, *Biointerphases*, 2008, **3**(1), IR1–IR5.

13 H. Huang, X. Sheng, Y. Tian, L. Zhang, Y. Chen and X. Zhang, Two-dimensional nanomaterials for anticorrosive polymeric coatings: a review, *Ind. Eng. Chem. Res.*, 2020, **59**(35), 15424–15446.

14 F. D'Souza and K. M. Kadish, *Handbook of Carbon Nano Materials*. World Scientific: 2014.

15 D. A. Brownson and C. E. Banks, *The handbook of graphene electrochemistry*, 2014.

16 S. C. Ray, Application and uses of graphene oxide and reduced graphene oxide. *Applications of graphene and graphene-oxide based nanomaterials*, 2015, pp. 39–55.

17 X. Huang, X. Qi, F. Boey and H. Zhang, Graphene-based composites, *Chem. Soc. Rev.*, 2012, **41**(2), 666–686.

18 Y. Zhu, S. Murali, W. Cai, X. Li, J. W. Suk, J. R. Potts and R. S. Ruoff, Graphene and graphene oxide: synthesis, properties, and applications, *Adv. Mater*, 2010, **22**(35), 3906–3924.

19 M. Pumera, Electrochemistry of graphene: new horizons for sensing and energy storage, *Chem. Rec.*, 2009, **9**(4), 211–223.

20 M. Khatamian, N. Khodakarampoor and M. Saket-Oskoui, Efficient removal of arsenic using graphene-zeolite based composites, *J. Colloid Interface Sci.*, 2017, **498**, 433–441.

21 S. Tkachev, E. Y. Buslaeva and S. Gubin, Graphene: A novel carbon nanomaterial, *Inorg. Mater.*, 2011, **47**(1), 1–10.

22 M. Khatamian, B. Divband and F. Farahmand-Zahed, Synthesis and characterization of Zinc (II)-loaded Zeolite/Graphene oxide nanocomposite as a new drug carrier, *Mater. Sci. Eng., C*, 2016, **66**, 251–258.

23 S. Stankovich, D. A. Dikin, R. D. Piner, K. A. Kohlhaas, A. Kleinhammes, Y. Jia, Y. Wu, S. T. Nguyen and R. S. Ruoff, Synthesis of graphene-based nanosheets via chemical reduction of exfoliated graphite oxide, *Carbon*, 2007, **45**(7), 1558–1565.

24 A. K. Hussain, I. Sudin, U. M. Basheer and M. Z. M. Yusop, A review on graphene-based polymer composite coatings for the corrosion protection of metals, *Corros. Rev.*, 2019, **37**(4), 343–363.

25 S. Liu, B. Yu and T. Zhang, Preparation of crumpled reduced graphene oxide–poly (p-phenylenediamine) hybrids for the detection of dopamine, *J. Mater. Chem. A*, 2013, **1**(42), 13314–13320.

26 Z. Huang, L. Li, Y. Wang, C. Zhang and T. Liu, Polyaniline/graphene nanocomposites towards high-performance supercapacitors: a review, *Compos. Commun.*, 2018, **8**, 83–91.

27 T. Wang, H. Sun, T. Peng, B. Liu, Y. Hou and B. Lei, Preparation and characterization of polyaniline/p-phenylenediamine grafted graphene oxide composites for supercapacitors, *J. Mol. Struct.*, 2020, **1221**, 128835.

28 Q. L. Pham, Y. Haldorai, N. Van Hoa, D. Tuma and J.-J. Shim, Facile synthesis of poly (p-phenylenediamine)/MWCNT nanocomposites and characterization for investigation of structural effects of carbon nanotubes, *Bull. Mater. Sci.*, 2011, **34**(1), 37–43.

29 J. Wei, T. Vo and F. Inam, Epoxy/graphene nanocomposites–processing and properties: a review, *RSC Adv.*, 2015, **5**(90), 73510–73524.

30 X. Shi, T. A. Nguyen, Z. Suo, Y. Liu and R. Avci, Effect of nanoparticles on the anticorrosion and mechanical properties of epoxy coating, *Surf. Coat. Technol.*, 2009, **204**(3), 237–245.

31 A. J. Dominis, G. M. Spinks and G. G. Wallace, Comparison of polyaniline primers prepared with different dopants for corrosion protection of steel, *Prog. Org. Coat.*, 2003, **48**(1), 43–49.

32 J. Fang, K. Xu, L. Zhu, Z. Zhou and H. Tang, A study on mechanism of corrosion protection of polyaniline coating and its failure, *Corros. Sci.*, 2007, **49**(11), 4232–4242.

33 T. Schauer, A. Joos, L. Dulog and C. Eisenbach, Protection of iron against corrosion with polyaniline primers, *Prog. Org. Coat.*, 1998, **33**(1), 20–27.

34 A. Hartwig, M. Sebald, D. Pütz and L. Aberle, in Preparation, characterisation and properties of nanocomposites based on epoxy resins–An overview, *Macromolecular symposia*, Wiley Online Library, 2005, pp 127–136.

35 O. Becker, R. Varley and G. Simon, Morphology, thermal relaxations and mechanical properties of layered silicate nanocomposites based upon high-functionality epoxy resins, *Polymer*, 2002, **43**(16), 4365–4373.

36 L. Yang, F. Liu and E. Han, Effects of P/B on the properties of anticorrosive coatings with different particle size, *Prog. Org. Coat.*, 2005, **53**(2), 91–98.

37 S. V. Lamaka, M. L. Zheludkevich, K. A. Yasakau, R. Serra, S. Poznyak and M. Ferreira, Nanoporous titania interlayer as reservoir of corrosion inhibitors for coatings with self-healing ability, *Prog. Org. Coat.*, 2007, **58**(2–3), 127–135.

38 A. Mostafaei and F. Nasirpouri, Electrochemical study of epoxy coating containing novel conducting nanocomposite comprising polyaniline–ZnO nanorods on low carbon steel, *Corros. Eng., Sci. Technol.*, 2013, **48**(7), 513–524.

39 A. Mostafaei and F. Nasirpouri, Preparation and characterization of a novel conducting nanocomposite blended with epoxy coating for antifouling and antibacterial applications, *J. Coat. Technol. Res.*, 2013, **10**(5), 679–694.

40 A. Mostafaei and F. Nasirpouri, Epoxy/polyaniline–ZnO nanorods hybrid nanocomposite coatings: Synthesis, characterization and corrosion protection performance of conducting paints, *Prog. Org. Coat.*, 2014, **77**(1), 146–159.

41 S. Pourhashem, M. R. Vaezi and A. Rashidi, Investigating the effect of SiO2-graphene oxide hybrid as inorganic nanofiller on corrosion protection properties of epoxy coatings, *Surf. Coat. Technol.*, 2017, **311**, 282–294.

42 Z. Yu, H. Di, Y. Ma, Y. He, L. Liang, L. Lv, X. Ran, Y. Pan and Z. Luo, Preparation of graphene oxide modified by titanium dioxide to enhance the anti-corrosion performance of epoxy coatings, *Surf. Coat. Technol.*, 2015, **276**, 471–478.

43 Z. Yu, H. Di, Y. Ma, L. Lv, Y. Pan, C. Zhang and Y. He, Fabrication of graphene oxide–alumina hybrids to reinforce the anti-corrosion performance of composite epoxy coatings, *Appl. Surf. Sci.*, 2015, **351**, 986–996.

44 S. Fazli-Shokouhi, F. Nasirpouri and M. Khatamian, Polyaniline-modified graphene oxide nanocomposites in epoxy coatings for enhancing the anticorrosion and antifouling properties, *J. Coat. Technol. Res.*, 2019, **16**(4), 983–997.

45 V. A. Mooss, A. A. Bhopale, P. P. Deshpande and A. A. Athawale, Graphene oxide-modified polyaniline pigment for epoxy based anti-corrosion coatings, *Chem. Pap.*, 2017, **71**(8), 1515–1528.

46 X. Sheng, W. Cai, L. Zhong, D. Xie and X. Zhang, Synthesis of functionalised graphene/polyaniline nanocomposites with effective synergistic reinforcement on anticorrosion, *Ind. Eng. Chem. Res.*, 2016, **55**(31), 8576–8585.

47 H. Wang, S. Wang, Y. Li, M. Li, Y. Xu, K. He, C. Yuan, B. Zeng and L. Dai, Fabrication of excellent anti-corrosion epoxy coating based on GON-An composites, *Surf. Eng.*, 2020, 1–12.

48 F. Nasirpouri, H. Pourmahmoudi, F. Abbasi, S. Littlejohn, A. S. Chauhan and A. Nogaret, Modification of chemically exfoliated graphene to produce efficient piezoresistive polystyrene–graphene composites, *J. Electron. Mater.*, 2015, **44**(10), 3512–3522.

49 B. Ramezanzadeh, S. Niroumandrad, A. Ahmadi, M. Mahdavian and M. M. Moghadam, Enhancement of

barrier and corrosion protection performance of an epoxy coating through wet transfer of amino functionalised graphene oxide, *Corros. Sci.*, 2016, **103**, 283–304.

50 H. Di, Z. Yu, Y. Ma, F. Li, L. Lv, Y. Pan, Y. Lin, Y. Liu and Y. He, Graphene oxide decorated with Fe3O4 nanoparticles with advanced anticorrosive properties of epoxy coatings, *J. Taiwan Inst. Chem. Eng.*, 2016, **64**, 244–251.

51 M. Li, W. Yin, X. Han and X. Chang, Hierarchical nanocomposites of polyaniline scales coated on graphene oxide sheets for enhanced supercapacitors, *J. Solid State Electrochem.*, 2016, **20**(7), 1941–1948.

52 F. Thema, M. Moloto, E. Dikio, N. Nyangiwe, L. Kotsedi, M. Maaza and M. Khenfouch, Synthesis and characterization of graphene thin films by chemical reduction of exfoliated and intercalated graphite oxide, *J. Chem.*, 2013, **2013**.

53 J. Sun and H. Bi, Pickering emulsion fabrication and enhanced supercapacity of graphene oxide-covered polyaniline nanoparticles, *Mater. Lett.*, 2012, **81**, 48–51.

54 V. V. Shunaev and O. E. Glukhova, Topology Influence on the process of graphene functionalisation by epoxy and hydroxyl groups, *J. Phys. Chem. C*, 2016, **120**(7), 4145–4149.

55 Y. Cao, H. J. Choi, W. L. Zhang, B. Wang, C. Hao and J. Liu, Eco-friendly mass production of poly (p-phenylenediamine)/ graphene oxide nanoplatelet composites and their electrorheological characteristics, *Compos. Sci. Technol.*, 2016, **122**, 36–41.

56 Y. Lu, Y. Huang, F. Zhang, L. Zhang, X. Yang, T. Zhang, K. Leng, M. Zhang and Y. Chen, Functionalised graphene oxide based on p-phenylenediamine as spacers and nitrogen dopants for high performance supercapacitors, *Chin. Sci. Bull.*, 2014, **59**(16), 1809–1815.

57 M. Kotal and A. K. Bhowmick, Multifunctional hybrid materials based on carbon nanotube chemically bonded to reduced graphene oxide, *J. Phys. Chem. C*, 2013, **117**(48), 25865–25875.

58 R. Shah, A. Kausar, B. Muhammad and M. Khan, Investigation on thermal conductivity and physical properties of polythiophene/p-phenylenediamine-graphene oxide and polythiophene-co-poly (methyl methacrylate)/p-phenylenediamine graphene oxide composites, *Compos. Interfaces*, 2016, **23**(9), 887–899.

59 Q. Yin, R. Shu, H. Xing, D. Tan, Y. Gan and G. Xu, Rheological behavior and electrical properties of graphene oxide/polyaniline nanocomposites, *Nano*, 2016, **11**(02), 1650020.

60 D. Chaudhuri and D. Sarma, BF 3-doped polyaniline: A novel conducting polymer, *Pramana*, 2006, **67**(1), 135–139.

61 H. Wei, J. Zhu, S. Wu, S. Wei and Z. Guo, Electrochromic polyaniline/graphite oxide nanocomposites with endured electrochemical energy storage, *Polymer*, 2013, **54**(7), 1820–1831.

62 X. Li, H. Song, Y. Zhang, H. Wang, K. Du, H. Li, Y. Yuan and J. Huang, Enhanced electrochemical capacitance of

graphene nanosheets coating with polyaniline for supercapacitors, *Int. J. Electrochem. Sci.*, 2012, **7**, 5163–5171.

63 Y. Zhao, G.-S. Tang, Z.-Z. Yu and J.-S. Qi, The effect of graphite oxide on the thermoelectric properties of polyaniline, *Carbon*, 2012, **50**(8), 3064–3073.

64 N. Yang, J. Zhai, M. Wan, D. Wang and L. Jiang, Layered nanostructures of polyaniline with graphene oxide as the dopant and template, *Synth. Met.*, 2010, **160**(15–16), 1617–1622.

65 M. Li, C. Liu, H. Cao, J. Pan, H. Zhao and Y. Zhang, The determination of surface charge on nitrogen-containing reduced graphene oxides and its application to adsorb molybdate, *Mater. Chem. Phys.*, 2015, **152**, 77–84.

66 C. Liu, Q. Bi, A. Leyland and A. Matthews, An electrochemical impedance spectroscopy study of the corrosion behaviour of PVD coated steels in 0.5 N NaCl aqueous solution: Part II.: EIS interpretation of corrosion behaviour, *Corros. Sci.*, 2003, **45**(6), 1257–1273.

67 T. T. X. Hang, T. A. Truc, T. H. Nam, V. K. Oanh, J.-B. Jorcin and N. Pébère, Corrosion protection of carbon steel by an epoxy resin containing organically modified clay, *Surf. Coat. Technol.*, 2007, **201**(16–17), 7408–7415.

68 S. Mohammadi, F. A. Taromi, H. Shariatpanahi, J. Neshati and M. Hemmati, Electrochemical and anticorrosion behavior of functionalised graphite nanoplatelets epoxy coating, *J. Ind. Eng. Chem.*, 2014, **20**(6), 4124–4139.

69 S. Pourhashem, A. Rashidi, M. R. Vaezi and M. R. Bagherzadeh, Excellent corrosion protection performance of epoxy composite coatings filled with amino-silane functionalised graphene oxide, *Surf. Coat. Technol.*, 2017, **317**, 1–9.

70 W. Sun, L. Wang, T. Wu, Y. Pan and G. Liu, Inhibited corrosion-promotion activity of graphene encapsulated in nanosized silicon oxide, *J. Mater. Chem. A*, 2015, **3**(32), 16843–16848.

71 H. Di, Z. Yu, Y. Ma, C. Zhang, F. Li, L. Lv, Y. Pan, H. Shi and Y. He, Corrosion-resistant hybrid coatings based on graphene oxide–zirconia dioxide/epoxy system, *J. Taiwan Inst. Chem. Eng.*, 2016, **67**, 511–520.

72 S. Mohammadi, H. Shariatpanahi, F. A. Taromi and J. Neshati, Electrochemical and anticorrosion behaviors of hybrid functionalised graphite nano-platelets/ tripolyphosphate in epoxy-coated carbon steel, *Mater. Res. Bull.*, 2016, **80**, 7–22.

73 M. Li, X. Ji, L. Cui and J. Liu, In situ preparation of graphene/ polypyrrole nanocomposite via electrochemical co-deposition methodology for anti-corrosion application, *J. Mater. Sci.*, 2017, **52**(20), 12251–12265.

74 B. Ramezanzadeh, Z. Haeri and M. Ramezanzadeh, A facile route of making silica nanoparticles-covered graphene oxide nanohybrids (SiO$_2$-GO); fabrication of SiO2-GO/epoxy composite coating with superior barrier and corrosion protection performance, *Chem. Eng. J.*, 2016, **303**, 511–528.